M. Teich, J. Sturm, L. Büttner, J. Czarske

Distortion-free 3D imaging using wavefront shaping

Erstveröffentlichung in / First published in:

SPIE Digital Optical Technologies. Munich, 2017. Bellingham: SPIE, Vol. 10335 *[Zugriff am: 02.05.2019]*.

DOI: https://doi.org/10.1117/12.2269928

Distortion-free 3D imaging using wavefront shaping

M. Teich, J. Sturm, L. Büttner, J. Czarske

M. Teich, J. Sturm, L. Büttner, J. Czarske, "Distortion-free 3D imaging using wavefront shaping," Proc. SPIE 10335, Digital Optical Technologies 2017, 1033514 (26 June 2017); doi: 10.1117/12.2269928

SPIE.

Event: SPIE Digital Optical Technologies, 2017, Munich, Germany

Distortion-free 3D-imaging using wavefront-shaping

M. Teich*, J. Sturm, L. Büttner, J. Czarske
Technische Universität Dresden, Fakultät Elektrotechnik und Informationstechnik, Professur für Mess- und Sensorsystemtechnik, Helmholtzstrasse 18, D-01069 Dresden

ABSTRACT

3-dimensional imaging often requires substantial effort since information along the optical axis is not straight forward gatherable. In many applications it is aimed for depth information along the direction of view. For example fluidic mixing processes and the environmental interaction on a microscopic scale are of particular importance for e.g. pharmaceutical applications and often demand for 3D information. This problem is often solved by stereoscopic approaches, where two cameras are used in order to gather depth information by triangulation technique. Another approach is to scan the object through the focal plane in order to get sharp images of each layer. Since the before mentioned approaches require a lot of video data to be evaluated it would be more convenient to get depth mapping within a single camera recording and without scanning. Here we present a tunable 3D depth-mapping camera technique in combination with dynamic aberration control. By using an incoherent light source, only one camera and a spatial light modulator (LCoS-SLM), it is a simply applicable and highly scalable technique. A double-helix point spread function (DH-PSF) is generated for light emerging from the observed focal plane. Each object appears as a double-image on the camera. Within the orientation of the double-image, depth information along the optical axis is encoded. By using an additional adaptive element (deformable mirror) the technique is combined with wide-field aberration correction. Here we combine a tunable 3D depth camera with dynamic aberration control in one imaging system.

Keywords: wave front shaping, 3D imaging, SLM, double-helix PSF, micro-fluidics

*martin.teich@tu-dresden.de; https://tu-dresden.de/ing/elektrotechnik/iee/mst

1. INTRODUCTION

Particle or marker trajectories on a microscopic scale are important for many applications in biomedicine and micro-fluidics. The trajectory reveals the interaction of the fluid with the surrounding environment, e.g. markers in a cell or cell constituents or for the analysis of blood constituents[1]. Fluorescent particles or markers tag specific functional parts of cell systems, whose interaction with the environment is highly relevant for the understanding of biological processes on the microscopic scale. Diffusion[2], directed motion[3] can be captured and evaluated. A device-oriented playground of measuring particle-environment interaction is the micro-fluidic channel. They can be designed to e.g. separate and sort particles and molecules based on their diffusion coefficients[4]. Micro-fluidic devices have the potential to provide easily applicable clinical diagnostics and pharmaceutical screening tests[1]. They are also capable of studying mixing processes on a microscopic scale using only a very small probe of the fluid under investigation[5]. Beside micro- and nano-fluidic applications surveillance systems exhibit a lag of depth mapping ability[6]. This problem can be solved by a stereoscopic approach by using two cameras to gather depth information with triangulation technique. Another possibility especially for microscopy is scanning the object through the focal plane[7] in order to get sharp images of each layer. But this is not suitable for every application. Both approaches require lot of video data. It would be more convenient to get depth mapping within a single camera recording i.e. without scanning or triangulation. Here we present a tunable 3D depth-mapping camera technique in combination with dynamic aberration control. It is a scan-free, fluorescence imaging technique for 3D trajectory and velocity measurement of flow fields[8]. By using an incoherent light source, only one camera and a spatial light modulator (LCoS-SLM) loaded with a spiral phase mask that generates double-images of the measurement object, it is a simply applicable and highly scalable technique[9]. A double-helix point spread function (DH-PSF)[10] is generated for light emerging from the observed focal plane. Each object appears as a double-image on the camera. Depth information along the optical axis is encoded within the orientation of the double-image. By using an additional adaptive element (deformable mirror), the technique is combined with wide-field aberration correction[11]. Here we combine a tunable 3D depth camera with dynamic aberration control in one imaging systems.

Digital Optical Technologies 2017, edited by Bernard C. Kress, Wolfgang Osten, H. Paul Urbach, Proc. of SPIE Vol. 10335, 1033514 · © 2017 SPIE
CCC code: 0277-786X/17/$18 · doi: 10.1117/12.2269928

2. OPTICAL SETUP AND DATA EVALUATION

This technique is a flexible and customizable way of modulating the phase of light in order to get depth information. The reflected light is phase-only modulated for one polarization direction by an LCoS-SLM. It generates a double-helix point spread function (DH-PSF) for light emerging from the focus. The light focus is situated in the focal plane of a microscope objective that is directed to a fluid flow that is seeded with fluorescent particle. Each light emitting particle appears as a double-image on the camera. Within the orientation of the double-image, depth information along the optical axis is decoded. A simple Gaussian mask fitting[12] algorithm is applied in order to identify the constituents of the double-images and particle tracking[12] results in the trajectory of the seeding particle and therefore the fluid flow velocity.

2.1 Experimental setup

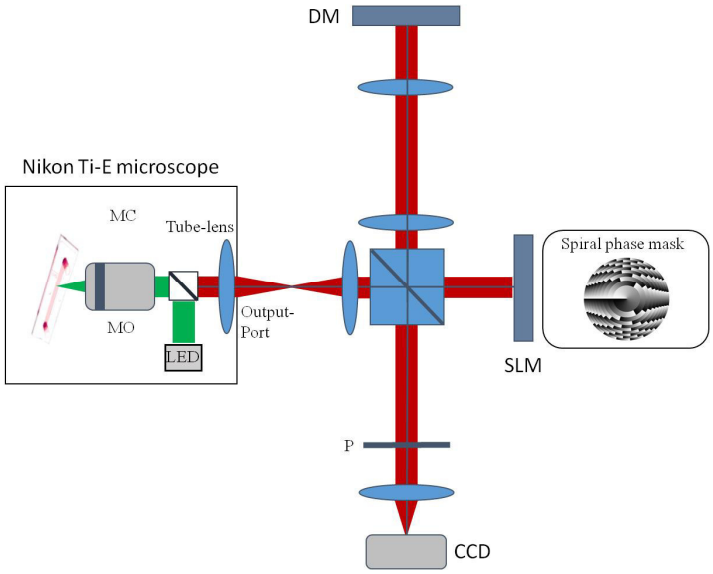

Figure 1. Experimental setup for 3D micro-channel (MC) fluid flow imaging with fluorescent seeding particles. Green light (532 nm) from a LED is focused through a microscope objective (MO) to the micro-channel. Fluorescent light (632 nm) is extracted via a chromatic beamsplitter and transferred to the microscope output port. A 3D-imaging setup is attached to the microscope containing an SLM loaded with a spiral phase mask, a deformable mirror for aberration correction and a CCD camera with a polarizer (P) in front.

As it is indicated in Figure 1, the setup consist of a Nikon Ti-E inverse microscope that is equipped with a high-power LED for the excitation of the seeding particles (microParticles GmbH polystyrol PS-FR-Fi256, 3.2 µm in diameter) in the micro-channel (self-made from PDMS on a glass plate, 100 µm channel thickness). A microscope objective (Nikon CFI plan S-Fluor 20x, NA=0.4) collects the light emitted from the seeding particles. An LCoS-SLM (Holoeye PLUTO-NIR-011 Phase Only, 1920x1080 pixel, 60 Hz) can be loaded with a spiral phase mask and additional aberrations (astigmatism and coma). A deformable membrane mirror (DM, OKOTech with 17 elements) is inserted after a telescope connecting the image planes of SLM and DM. A CCD camera (Basler camera pilot piA640-210gm, 648x488 pixel, 7.4 µm pitch, 210 Hz full-frame rate) records the fluid flow which can be precisely controlled (several µl/s) by a low pressure syringe pump (Cetoni) that is connected to the micro-channel. A polarizer selects the orientation for phase-only operation of the SLM.

2.2 Double-Helix Point Spread Function

The change in orientation angle dψ with the distance change dz along the optical axis can be expressed for a spiral phase mask in the following way[13]

$$\frac{d\psi}{dz} = \frac{\pi(NA)^2}{\lambda N \Delta l} \tag{1}$$

Important parameters are the numerical aperture NA (0.4) of the optical system, the used wavelength λ (632 nm, fluorescence emission), the number of radial zones N and the topological charge between neighboring zones Δl on the phase mask (see also inset in Figure 1). For Δl=2 a double-image is generated. For increasing N the separation of the Gaussian spots increases while the overall contrast is reduced due to limited phase-modulating area of the LCoS-SLM. The spiral phase mask can be optimized by varying parameter N for a certain particle size, magnification and SNR of the optical system in order to get optimal contrast for the double-images.

2.3 Software

Evaluating double-images of seeding particles means the analysis with a Gaussian mask fitting procedure. The image is scanned for Gaussian intensity distributions. The recognized intensity distributions are assigned to a particle. For 3D-PTV each particle is represented by a double-image of two Gaussian intensity distributions. By attributing two closely located Gaussian intensity distributions to one particle and analyzing the orientation of the double-image, the z-coordinate is extracted additionally to the x- and y- coordinates. Therefore full 3D information on the particle location is gathered. While performing this procedure frame by frame through all frames of the recorded video, the velocity directionality of the fluid flow is determined in 3 dimensions. For data evaluation we modified the open-source MATLAB plugin "PTVlab" developed by Antoine Patalano and Brevis Wernher [12].

3. MICROCHANNEL FLOW MEASUREMENTS

In Figure 2 is depicted a flow velocity measurement along the optical axis in a 100 µm thick micro-channel. Two different syringe pump flow rate have been applied with a factor of 2 in between (0.025 µl/s and 0.05 µl/s). Each data point (yellow and blue, respectively) indicates one velocity value measured within a recorded video of 55 seconds which corresponds to 2200 frames for a video frame rate of 40 Hz. In average 4 to 6 particles have been visible at once within the field of view. The measurement was taken with a 20x microscope objective with an NA of 0.4. Considering Equation 1 this leads to a theoretic measurement depth range of about 80 µm for a spiral phase mask of Δl=2 and N=5. The raw data points have been averaged within small depth range windows and mean values of the velocity along the optical axis have been plotted. For the averaged data points (red dots in Figure 2) a parabolic fit has been applied. The width of the parabola (velocity drop to zero) corresponds to the channel-width. For doubling the syringe pump rate the peak velocity (parabola maximum) doubles.

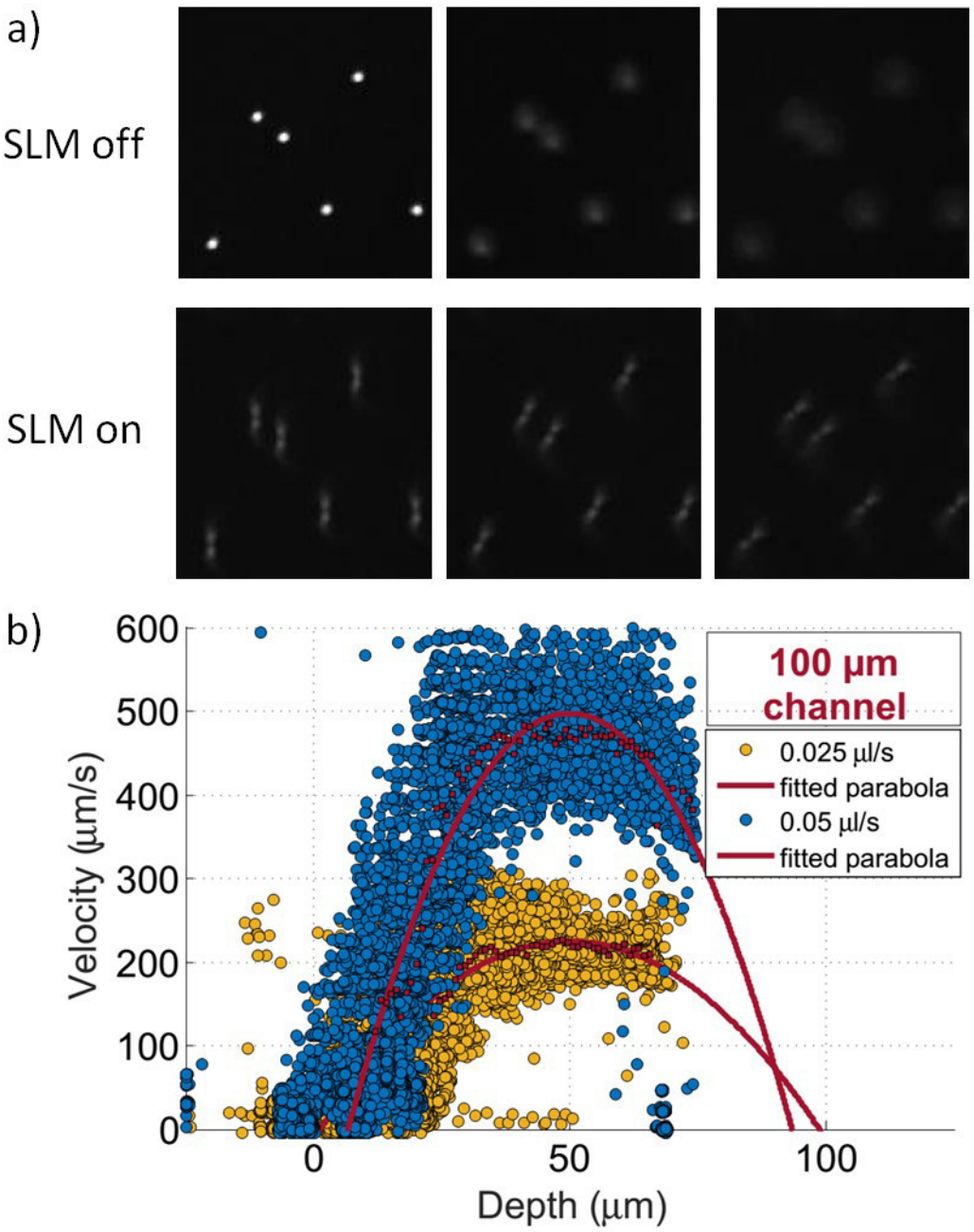

Figure 2. a) Exemplary images of the fluorescent seeding particles in a fluid flow with SLM off and on. For SLM-off the image is distorted by blurring. For SLM-on the defocus behavior is transformed into the rotation of double-images. b) Measurement of the z-component (i.e. along the optical axis) of the flow velocity within a 100 µm thick micro-channel for two different pump rates (0.025 µl/s and 0.05 µl/s). The parabolas were fitted to the mean values (red dots) within the standard deviation for each data set.

4. INFLUENCE OF ABBERATIONS

The influence of frequently emerging aberrations on the double-helix point spread function have been investigated theoretically[14] and experimentally[15,16,17] in the past. Beside spherical aberration usually occurring in the case of high-NA microcope objectives (immersion fluid) also astigmatism and coma play a significant role in optical imaging systems. Therefore we investigate the influence of 0° and 45° astigmatism as well as X and Y oriented coma on the double-helix point-spread function and try to estimate the impact on the velocity measurement that is performed by particle-tracking.

4.1 Astigmatism

Let us consider an optical distortion in form of astigmatism over the whole field of view. Then the wave aberration function can be written as follows[14]:

$$W(x,y) = -\frac{kA_{ax}}{R_0^2}x^2 \tag{2}$$

$$W(x,y) = -\frac{kA_{ay}}{R_0^2}y^2 \tag{3}$$

Here k is the wave vector, R_0 the radius of the optical system aperture and A_{ax}, A_{ay} the astigmatism coefficients (amplitudes). Considering the field of view on the camera as an XY-plane for X as the horizontal and Y as the vertical axis, then 0° astigmatism corresponds to a pure X-component (horizontal) and 45° astigmatism contains a mixture of X and Y component (diagonal), see also Figure 3. In Figure 3(b) is shown the influence on the double-image for applied astigmatism that was added to the spiral phase mask on the SLM. A positive (max) and a negative (min) amplitude value has been set for each configuration. The reference image shows 4 fluorescent particles that appear as double-images. Apparently all 4 particles are situated in the same depth along the optical axis (there orientation is almost equal). By applying 0° astigmatism both spots of the double-images become elliptically shaped along the X axis (horizontal). The orientation of the double-image i.e. the intensity maxima has changed for all 4 cases. This effect leads to a significant change in the calibration curve (angle against depth) shown in Figure 4. For 0° astigmatism, a strong positive and negative curvature is observed for negative (min) and positive (max) amplitude, respectively. This can be seen more clearly in the plot of the angle difference below the calibration curves in Figure 4. For 45° astigmatism, the curvature changes after the focal plane ($z/z_R=0$) because it is a mixture of X and Y contribution. The impact on flow velocity measurements is that for dynamically changing astigmatism new calibration curves have to be captured and exact look-up table have to be generated in order to attribute the correct particle depth to its double-image orientation. Otherwise the measured parabolic flow profile would be distorted along the depth position for each velocity value.

4.2 Coma

Another case of commonly emerging aberrations in optical systems is coma[14]. In that case the wave aberration function can be written in the following way:

$$W(x,y) = \frac{kA_{cx}}{R_0^3}x(x^2+y^2) \tag{4}$$

$$W(x,y) = \frac{kA_{cy}}{R_0^3}y(x^2+y^2) \tag{5}$$

Here similar to Equation 2 and 3, k is the wave vector, R_0 the radius of the optical system aperture and A_{cx}, A_{cy} the coma coefficients. Note that W depends in cubic form on R_0 and the influence of X coma is not independent from y axis and vice versa. As we have measured, coma does not affect the calibration angle versus depth (not shown here). This

behavior has already been demonstrated in numerical simulations[14] treating the influence of coma on the DH-PSF and confirming our findings. In Figure 5(b) is shown the influence of X and Y coma on the 4 particles that are recorded as double-images. Note that the expectable coma tail is a mixture of x and y axis contribution. Except for the case of Y coma with min and max amplitude where the coma tail is oriented along the y axis because the double-image itself has an orientation along the y axis. Notably is, that only one spot of the double-image is effected which is not observable for X coma where both spots get a coma tail. Beside the arising coma tail, the main effect is a center shift of the double images. This behavior is plotted in Figure 6. With increasing distance from the focal plane the center shift is getting stronger. For X coma the strongest influence is on the x center coordinate of the particle, but also the y coordinate is influenced. The main impact on velocity measurements is that the exact particle position in xy-plane is deteriorated. Supposing that the coma aberration does not change during the measurement time, this leads to a systematic coordinate offset for all particles within the field of view. Since the velocity is determined by the particle motion, the absolute xy-position is not so much important, especially when measuring along z-axis where the orientation of the double-image is the evaluated parameter.

In conclusion, as long as the aberration is static, the influence of astigmatism can be compensated by re-calibrating the system (look-up table) for the z coordinate. In case of coma the measurement of the velocity along the optical axis is not affected whereas the velocity field in xy-plane suffers from a position offset for the tracked particle and therefore a deformation of the 2D flow field is expected.

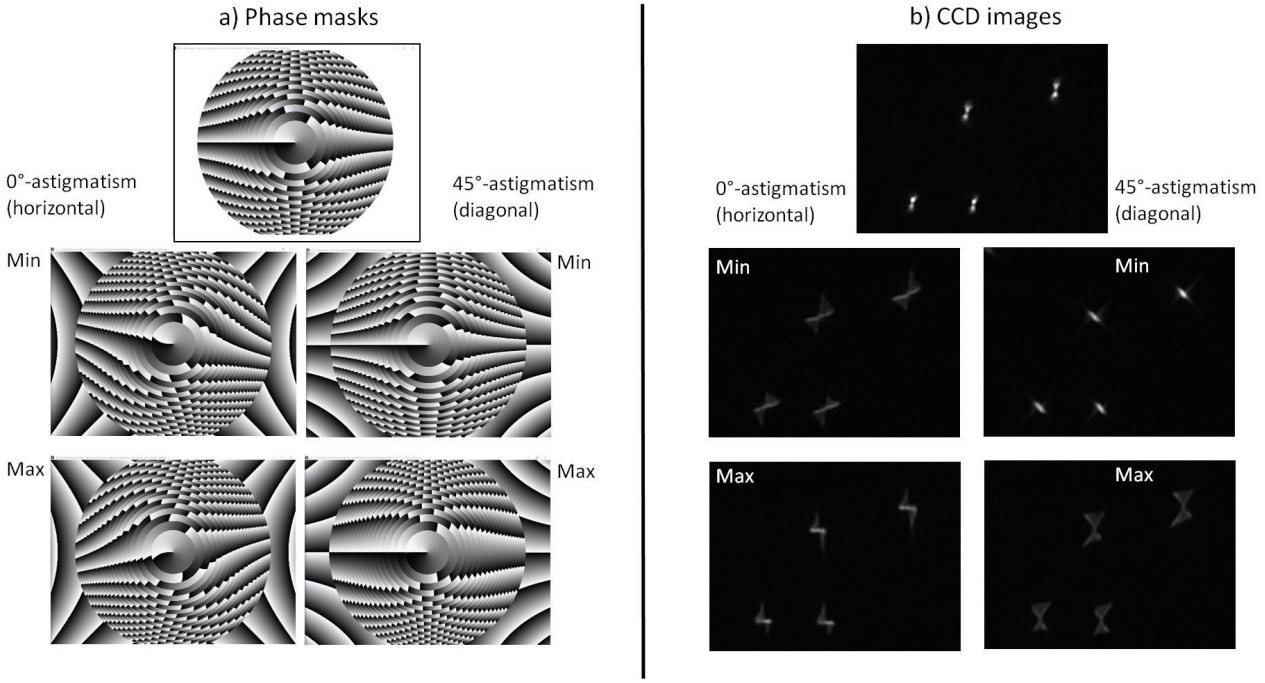

Figure 3. a) Additionally to the spiral phase mask, astigmatism was added to the SLM, here shown for 0° and 45° with a minimal (-) and a maximal (+) value. b) The double-image shape of the fluorescent seeding particles is deteriorated by the added astigmatism. The circular spot centers deform to an elliptic shape in the direction of the applied astigmatism.

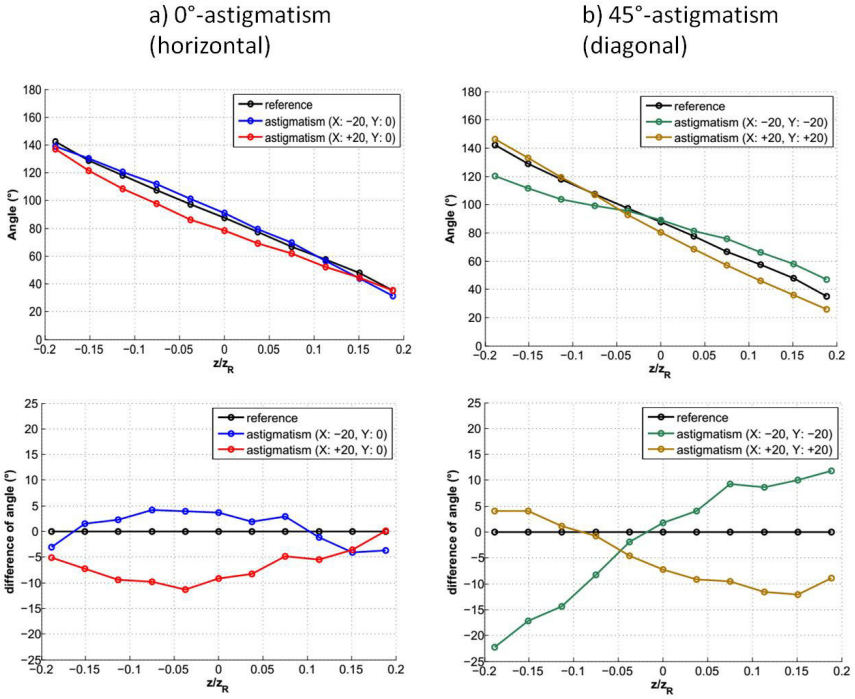

Figure 4. Effect of astigmatism on the calibration curve of the double-helix point spread function for 0° astigmatism (left) and 45° astigmatism (right). The effect of additional curvature within the calibration curve can be seen in the plot of angle difference below the calibration plots. The distance along the optical axis is plotted in terms of z/z_R where z_R is the Rayleigh length of the focus.

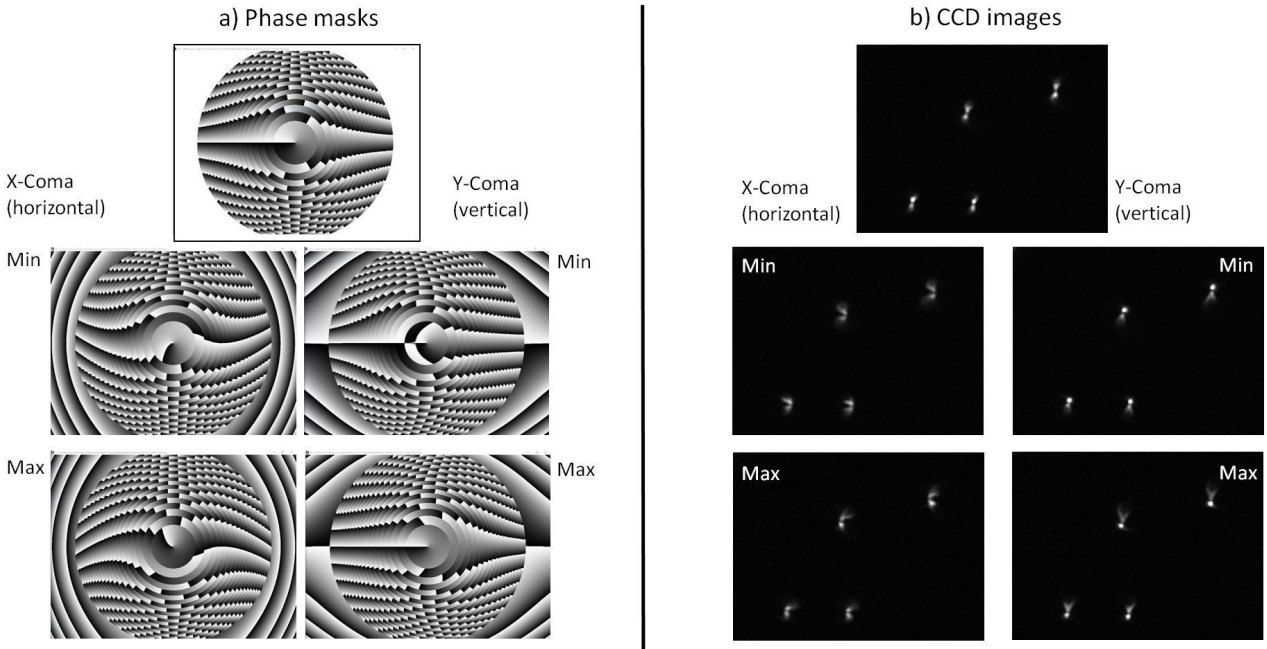

Figure 5. a) Additionally to the spiral phase mask, coma was added to the SLM, here shown for X and Y direction with a minimal (-) and a maximal (+) value. b) The double-image shape of the fluorescent seeding particles is deteriorated by the added coma. The circular spot centers change their shape to a coma tail in the direction of the applied coma. Note that for Y-Coma only one spot of the double-image is affected (upper for max and lower for min).

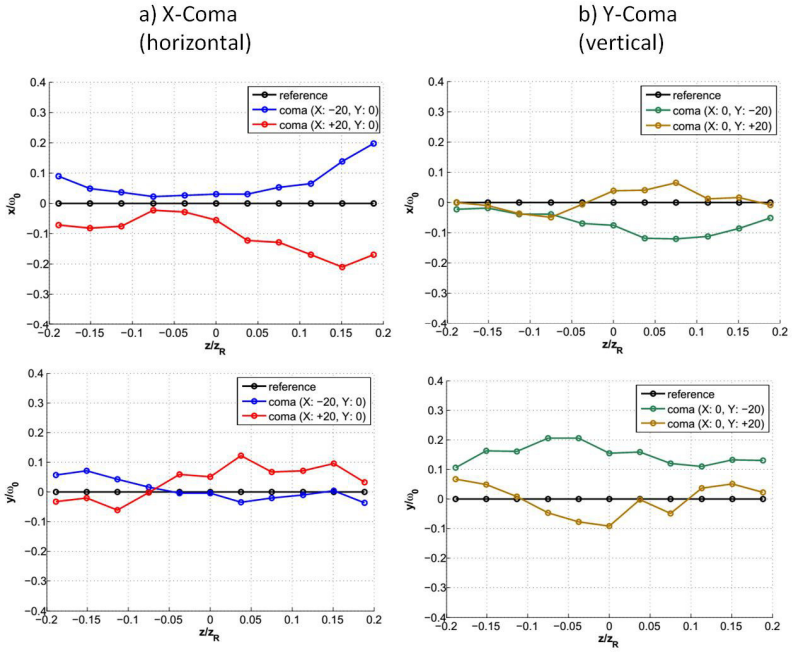

Figure 6. Effect of coma on the calibration curve of the double-helix point spread function for X (left) and Y (right) orientation. The effect of the center-shift on the double-image can be seen in the x/w_0 and y/w_0 coordinate plot (w_0: beam waist) against the distance from the focal plane along the optical axis, which is plotted in terms of z/z_R, where z_R is the Rayleigh length of the focus.

REFERENCES

[1] Xavier, M., Rosendahl, P., Herbig, M., Kräter, M., Spencer, D., Bornhäuser, M., Oreffo, R. O. C., Morgan, H., Guck, J., et al., "Mechanical phenotyping of primary human skeletal stem cells in heterogeneous populations by real-time deformability cytometry.," Integr. Biol. (Camb)., 10–12 (2016).

[2] Kamholz, A. E., Schilling, E. A.., Yager, P., "Optical measurement of transverse molecular diffusion in a microchannel.," Biophys. J. **80**(4), 1967–1972 (2001).

[3] Shechtman, Y., Weiss, L. E., Backer, A. S., Sahl, S. J.., Moerner, W. E., "Precise Three-Dimensional Scan-Free Multiple-Particle Tracking over Large Axial Ranges with Tetrapod Point Spread Functions," Nano Lett. **15**(6), 4194–4199 (2015).

[4] Brody, J. P.., Yager, P., "Diffusion-based extraction in a microfabricated device," Sensors Actuators A Phys. **58**(1), 13–18 (1997).

[5] Munson, M. S.., Yager, P., "Simple quantitative optical method for monitoring the extent of mixing applied to a novel microfluidic mixer," Anal. Chim. Acta **507**(1), 63–71 (2004).

[6] Berlich, R., Bräuer, A.., Stallinga, S., "Single shot three-dimensional imaging using an engineered point spread function," Opt. Express **24**(6), 5946 (2016).

[7] Philipp, K., Smolarski, A., Koukourakis, N., Fischer, A., Stürmer, M., Wallrabe, U.., Czarske, J. W., "Volumetric HiLo microscopy employing an electrically tunable lens," Opt. Express **24**(13), 15029 (2016).

[8] Teich, M., Mattern, M., Sturm, J., Büttner, L.., Czarske, J. W., "Spiral phase mask shadow-imaging for 3D-measurement of flow fields," Opt. Express **24**(24), 27371–27381 (2016).

[9] Quirin, S.., Piestun, R., "Depth estimation and image recovery using broadband, incoherent illumination with engineered point spread functions [Invited].," Appl. Opt. **52**(1), A367-76 (2013).

[10] Pavani, S. R. P.., Piestun, R., "Three dimensional tracking of fluorescent microparticles using a photon-limited double-helix response system.," Opt. Express **16**(26), 22048–22057 (2008).

[11] Warber, M., Maier, S., Haist, T.., Osten, W., "Combination of scene-based and stochastic measurement for wide-field aberration correction in microscopic imaging.," Appl. Opt. **49**(28), 5474–5479 (2010).

[12] Brevis, W., Niño, Y.., Jirka, G. H., "Integrating cross-correlation and relaxation algorithms for particle tracking velocimetry," Exp. Fluids **50**(1), 135–147 (2011).

[13] Baránek, M.., Bouchal, Z., "Optimizing the rotating point spread function by SLM aided spiral phase modulation," Spie **9441**, 94410N (2014).

[14] Cao, Z.., Wang, K., "Effects of astigmatism and coma on rotating point spread function," Appl. Opt. **53**(31), 7325–7330 (2014).

[15] Ghosh, S.., Preza, C., "Characterization of a three-dimensional double-helix point-spread function for fluorescence microscopy in the presence of spherical aberration.," J. Biomed. Opt. **18**(3), 36010 (2013).

[16] Baránek, M., Bouchal, P., Šiler, M.., Bouchal, Z., "Aberration resistant axial localization using a self-imaging of vortices," Opt. Express **23**(12), 15316 (2015).

[17] Koukourakis, N., Fregin, B., König, J., Büttner, L.., Czarske, J. W., "Wavefront shaping for imaging-based flow velocity measurements through distortions using a Fresnel guide star," Opt. Express, Vol. 24, Issue 19, pp. 22074-22087 **24**(19), 22074–22087 (2016).